Multiorbital effects in strong-field ionization and dissociation of aligned polar molecules CH_3I and CH_3Br

Sizuo Luo,[1] Shushan Zhou,[1] Wenhui Hu,[1] Xiaokai Li,[1] Pan Ma,[1] Jiaqi Yu,[1] Ruihan Zhu,[2] Chuncheng Wang,[1] Fuchun Liu,[1] Bing Yan,[1] Aihua Liu,[1] Yujun Yang,[1] Fuming Guo,[1,*] and Dajun Ding[1,†]

[1]*Institute of Atomic and Molecular Physics, Jilin Provincial Key Laboratory of Applied Atomic and Molecular Spectroscopy, Jilin University, Changchun 130012, China*

[2]*School of Science, Changchun University of Science and Technology, Changchun 130022, China*

(Received 18 December 2016; published 19 December 2017)

Controlling the molecular axis offers additional ways to study molecular ionization and dissociation in strong laser fields. We measure the ionization and dissociation yields of aligned polar CH_3X (X = I, Br) molecules in a linearly polarized femtosecond laser field. The current data show that maximum ionization occurs when the laser polarization is perpendicular to the molecular C-X axis, and dissociation prefers to occur at the laser polarization parallel to the C-X axis. The observed angular distributions suggest that the parent ions are generated by ionization from the HOMO. The angular distribution of fragment ions indicates that dissociation occurs mainly from an ionic excited state produced by ionization from the HOMO-1.

DOI: 10.1103/PhysRevA.96.063415

I. INTRODUCTION

Ionization is considered the first step when a strong laser field interacts with molecules and a trigger for subsequent dynamic processes, such as laser-induced electron diffraction [1,2], high-harmonic generation [3,4], and Coulomb explosion [5,6], which are important for understanding strong-field molecular physics and developing technologies for ultrafast imaging of molecular orbital and structure. Recently, various studies have shown that the single-active-electron (SAE) approximation cannot be translated well to describe the strong-field ionization and dissociation of multielectron polyatomic molecules [7–10]; the multiple orbital contribution is required to illustrate many phenomena [9–11]. Experimentally, observing the contribution of tunneling ionization from low-lying orbitals and disentangling the different symmetry and dynamics of multiple orbitals upon ionization and dissociation require advanced techniques based on molecular alignment [12–14] and coincidence measurement [15–18].

The measurement of angular-dependent strong-field ionization and dissociation yields reveals the contribution of multiple orbitals in the molecular frame [10,11]. Previous studies demonstrate that the angular-dependent yields of parent ions for N_2, O_2, and CO_2 molecules provide a possibility to image highest occupied molecular orbitals (HOMOs) [12,13], but the results give an angular distribution of the ionization from CO_2 very different from the theoretical prediction using the conventional Molecular Ammosov-Delone-Krainov method based on the single-active-electron approximation. This discrepancy has been assigned to the contribution of dynamics exchange [19]. Similarly, ionization of the polar OCS molecule has attracted intensive attention. Holmegaard *et al*. measured the photoelectron angular distributions of oriented OCS molecules in a circularly polarized laser; they showed that the discrepancy between the calculated and the observed ionization asymmetries may be attributed to the neglect of the Stark effect in the theoretical treatment [20]. Hansen *et al*. also observed that the ionization yields cannot reflect the shape of the single active orbital for OCS molecules and the obtained angular distribution of the parent ion cannot be reproduced by theory even with a Stark-shift correction [21]. Different methods have been used to reproduce the observations, such as the weak-field asymptotic theory [22] and adiabatic strong-field approximation (SFA) with orbital distortion [23]. Johansen *et al*. measured the angular distribution of OCS using a midinfrared laser; they also found the discrepancy between theory and experiment [24], and the calculation could be improved by including the alignment-dependent saturation factor but still could not reproduce the results under a high laser intensity. These attempts are far from satisfactory to reproduce the experimental observation of OCS molecules. The participation of excited states has been put forward to explain the deviation, which is difficult to include in the calculations. Moreover, it is found that the Stark effect and dynamic core polarization have a large influence in the case of polar molecules [25–27]. The orbital distortion contribution induced by the Stark effect has also been observed for the polar molecules CH_3F and CH_3Br [28] recently, and Walt *et al*. demonstrated the Stark effect and multielectron effects to be important in strong-field ionization and fragmentation of polar molecules CH_3X (X = F, Cl, Br, I) [29]. Therefore, these studies indicate that the angular distribution of strong-field ionization of polar molecules with degenerate asymmetric π orbitals is an interesting test for theoretical calculations.

Though single-active-electron theories of molecular ionization can contribute to the identification of new angular-resolved phenomena in tunneling ionization [10–12,19–21], a fundamental issue that has received extensive attention is related to the role of the multiorbital effect in strong-field molecular ionization and dissociation. For many molecules, strong-field dissociation occurs via the excited states of molecular ions generated either by tunneling ionization from low-lying orbital or by postionization excitation from ionic states of molecules [11,14–18]. The distinction of these two

*guofm@jlu.edu.cn
†dajund@jlu.edu.cn

 ©2017 American Physical Society

excitation pathways also relates to the ionization mechanisms of molecules, such as tunneling ionization at high laser intensities and multiphoton ionization at lower laser intensities. In the tunneling ionization regime, Akagi *et al*. found that both the HOMO and the HOMO-1 contribute to producing fragment ions Cl^+ and H^+ from HCl molecules, and the HOMO has an important influence on dissociation when laser polarization is perpendicular to the direction of the molecular axis [11]. Xie *et al*. performed measurements of alignment-dependent evolutions of C_2H_2 parent and fragment ions [14]. The observed evolutions show that the parent ion is generated by tunneling ionization from the HOMO but the fragment ions are produced from low-lying orbitals. Wu *et al*. studied the contribution of the HOMO to the next two lower-lying molecular orbitals in dissociation and Coulomb explosion of CO molecules from measurement of the orientation-dependent yields of fragment ions [15]. On the other hand, several other experiments at lower laser intensities show that postionization excitation makes an important contribution to the angular distribution of fragment ions [16–18], in which the molecule first is ionized from its HOMO and then absorbs extra photons for the transition to ionic excited states. Sándor *et al*. [17] and Zhao *et al*. [18] measured multiorbital contributions to the strong-field ionization and dissociation of several molecules by using coincident electron spectroscopy. Their results indicated that fragment ions can be generated by both ionization from a lower-lying orbital and the HOMO. The contribution of these two pathways is also determined by the energy gap between nondissociative and dissociative states involved in molecular dissociation; for example, when the energy gap is smaller than the energy of one photon, these two pathways are comparably important, and if the energy gap is larger than the energy of one photon, postionization excitation is dominant. All of these findings suggest that the multiorbital contribution plays an important role in complex ionization and dissociation dynamics of molecules in strong laser fields.

In this work, we measure the angular-dependent yields of ionization and dissociation from CH_3X (X = I, Br) by controlling the alignment of molecules using a nonresonant femtosecond laser to investigate the contribution of asymmetric π-orbital and multiorbital effects on ionization and dissociation of polar molecules in strong laser fields. The results demonstrate that the ionization of different orbitals correspond to the formation of parent and fragment ions. To identify the contributions of different molecular orbitals, discussion is also presented based on these observations together with some theoretical simulations.

II. EXPERIMENTAL AND THEORETICAL METHODS

The experimental setup is schematically described in Fig. 1(a) and is similar to that used in our previous studies [30–32]. The experiments utilize a Ti:sapphire laser to produce 50-fs, 800-nm linearly polarized laser pulses with an energy of up to 4 mJ at a 1-kHz repetition rate. A Mach-Zehnder interferometer is constructed to split the laser beam into two parts for pump-probe measurement, and the intensities of both parts are variable with the use of a half-wave plate and a Glan polarizer. In order to achieve a high degree of alignment without significant ionization, a pump pulse passes through a

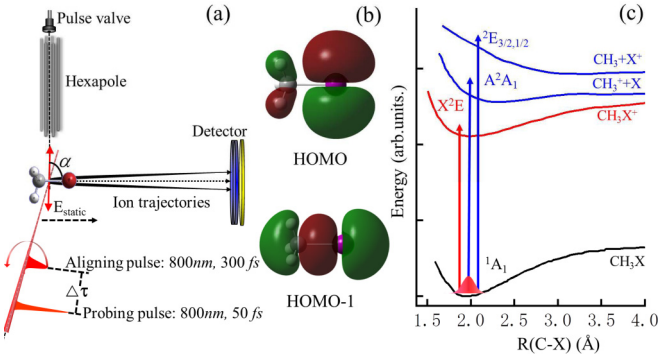

FIG. 1. (a) Pump-probe scheme for measuring the alignment-dependent ionization of CH_3X (X = I, Br) molecules. (b) HOMO and HOMO-1 of the CH_3I molecule. (c) Schematic of ionization and fragmentation pathways and relevant energy levels of CH_3X (X = I, Br) molecules; colored arrows indicate directly tunneling ionization from different orbitals.

piece of 70-mm BK7 glass to stretch it to approximately 300 fs. The spot size of the pump beam is reduced by using an aperture to ensure that its focus is larger than that of the probe beam. The probe beam is sent through a computer-controlled delay stage and a half-wave plate rotates the laser polarization. The pump and probe pulses are collinear and focused with a 250-mm-focal-length lens onto the molecular beam. The spectrometer contains three sections: a source chamber, a hexapole chamber, and a velocity-map-imaging chamber. In the source chamber, the supersonic molecular beam is produced by a pulsed valve (General Valve series 9) with 2.5% CH_3I or CH_3Br seeded in neon at a 4-b stagnation pressure through a 0.5-mm orifice. In the hexapole chamber, a 1-m hexapole rotational-state selector, composed of six hexagonally placed rods of 4-mm diameter, is used to prepare a specific rotational-state-selected molecular beam for the purpose of achieving a high degree of alignment. The CH_3X molecules after the selector are mainly populated at $|J,K,M\rangle = |1,\pm1,\pm1\rangle$ rotational states. The alignment of these rotational-state-selected molecules has been studied perviously [31,32]; the nonresonant laser (the pump beam) interacts with these state-selected molecules and the obtained maximum degree of alignment is $\langle\cos^2\theta\rangle = 0.7$. These well-aligned molecules are used as the targets for measuring the angular-dependent ionization yields in the strong laser field (the probe beam). The ions generated by the laser field are extracted and accelerated by an electrostatic lens system and are projected onto a detector at the end of a time-of-flight tube. The mass spectra can be obtained with a photomultiplier tube, accumulated and averaged by a digital storage oscilloscope, and, finally, transferred into a computer. The intensity of the femtosecond laser is calibrated by the saturated intensity of Xe ionization [33].

The SFA [20,23,34,35] and time-dependent density functional theory (TDDFT) [36,37] methods have been widely applied to describe molecular ionization in strong laser fields. In order to explain the experimental results, we performed calculation of the angular-dependent ionization rates using the molecular strong-field approximation (MO-SFA) method [34,35]. The SFA method treats the Coulomb potential in a perturbative way and the external laser field in a

nonperturbative way after ionization and has the advantage of calculating the ionization rate from multiphoton to tunneling ionization. The transition amplitudes of ionization for molecules at the length gauge can be written as

$$f_\alpha(\vec{p}) = -i \int_{-\infty}^{+\infty} \langle \vec{p} + \vec{A}_\alpha(t) | \vec{E}(t) \cdot \vec{r} | \varphi_0 \rangle e^{-iS_\alpha(\vec{p},t)} dt, \quad (1)$$

where

$$S_\alpha(\vec{p},t) = \int_t^{+\infty} [\vec{p} + \vec{A}_\alpha(t')]^2/2 + I_p, \quad (2)$$

with

$$|\vec{p} + \vec{A}_\alpha(t)\rangle = 1/(2\pi)^{3/2} e^{i[\vec{p}+\vec{A}_\alpha(t)]\cdot\vec{r}}, \quad (3)$$

and φ_0 is the molecular orbital function, $\vec{E}(t)$ is the laser electric field, $\vec{A}_\alpha(t)$ is the vector potential of the laser field, $\vec{p}$ is the momentum of the electron, and I_p is the ionization potential of the molecule. The ionization yield for molecules at different angles α can be given by

$$P(\alpha) = \int |f_\alpha(\vec{p})|^2 dp^3. \quad (4)$$

The wave function φ_0 of the molecular orbital in the MO-SFA calculation is obtained using GAMESS software with the basis set SPK-QZP [38]. Schematics of the HOMO and HOMO-1 of CH_3I molecules are shown in Fig. 1(b). Different orbital wave functions are used in calculating the ionization rates from the HOMO and HOMO-1. A schematic of the ionization and dissociation pathways is shown in Fig. 1(c). The fragment ions are generated by dissociation of excited molecular ions. These ions further are dissociated either into CH_3^+ and X (I, Br) when populated in the $A\,^2A_1$ state or into CH_3 and X^+ (X = I, Br) when populated in the $E_{3/2,1/2}$ state [39,40].

Alternatively, the TDDFT method is also used to calculate molecular ionization rates because it naturally includes multielectron dynamics [36,37]. We calculate the angular-dependent multiorbital ionization rates of CH_3X by employing a set of time-dependent Kohn-Sham (TDKS) equations to construct the evolutions of electron density in laser fields. The TDKS equations are

$$i\frac{\partial}{\partial t}\Psi_i(r,t) = \left[-\frac{\nabla^2}{2} + V_{\text{eff}}(r,t)\right]\Psi_i(r,t) \quad (i = 1,2,\ldots,N), \quad (5)$$

where $\Psi_i(r,t)$ is the Kohn-Sham orbital, N is the number of orbitals, and the time-dependent Kohn-Sham potential $V_{\text{eff}}(r,t)$ is

$$V_{\text{eff}}(r,t) = V_{\text{ne}}(r) + V_H(r,t) + V_{\text{xc}}(r,t) + r \cdot E(t), \quad (6)$$

where V_{ne} is the electron-nuclear potential, V_H is the Hartree potential, and V_{xc} is the exchange-correlation potential, which all include the multielectron effect, and the local density approximation has been used to construct the exchange-correlation potential, $E(t)$ is the electric field of the laser, which is a trapezoidal field in our calculation. Different pseudopotentials have been used to represent the electron-ion interaction of atoms, the electron-ion interaction for the C atom is represented by norm-conserving Troullier-Martins pseudopotentials [41], and those for the H, Br, and I atoms

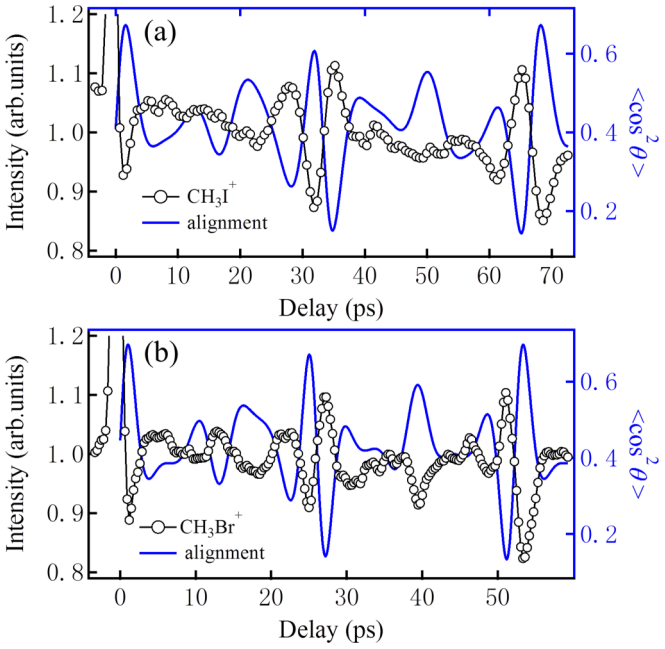

FIG. 2. Measured parent ion yields of CH_3I^+ and CH_3Br^+ as a function of the pump-probe delay. Black circles represent the alignment-dependent yield; blue lines, the time-dependent alignment evolution $\langle\cos^2\theta\rangle$ calculated by the time-dependent Schrödinger equation.

are represented by Hartwigsen-Goedecker-Hutter pseudopotentials [42]. The TDKS equations are calculated by using OCTOPUS [43,44]; the time-dependent survival probability of a particular Kohn-Sham orbital is

$$N_i(t) = \int |\Psi_i(r,t)|^2 dr, \quad (7)$$

and the ionization probability of a particular Kohn-Sham orbital is

$$P_i(t) = 1 - N_i(t). \quad (8)$$

The angular distribution of multiorbital ionization is the ionization probability obtained from different angles between the laser field $E(t)$ and the molecular axis.

III. RESULTS AND DISCUSSION

We measured the alignment dependence and angular distributions of parent and fragment ions of polar molecules CH_3X (X = I, Br). The alignment-dependent ionization yields are shown in Fig. 2, in which the measured time evolution of the parent ion CH_3I^+ and CH_3Br^+ signal intensity is shown by the black circles and the calculated time evolution of alignment $\langle\cos^2\theta\rangle$ by the blue lines. The degree of alignment is calculated using the time-dependent Schrödinger equation [45]. It is clearly shown that the time evolutions of parent ion yields are out of phase by π with respect to the time evolutions of alignment, indicating that CH_3I and CH_3Br prefer to be ionized when the probe laser polarization is perpendicular to the molecular axis. In Fig. 2, we also see that, in order to measure the angular-dependent ionization yield of CH_3X, the probe laser interacts with the molecules at a delay time

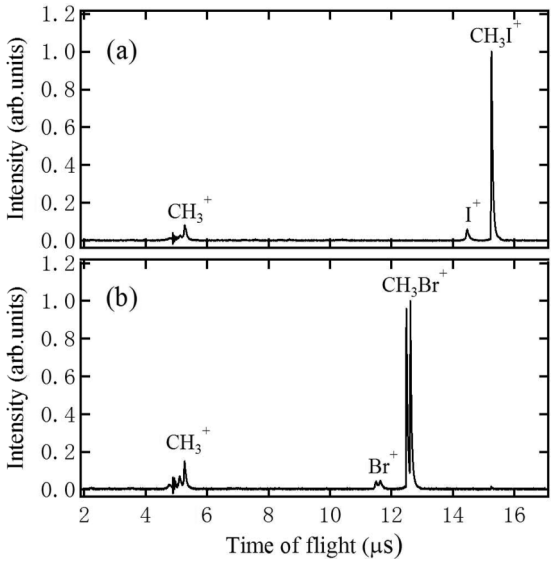

FIG. 3. Time-of-flight mass spectra of (a) CH_3I and (b) CH_3Br irradiated with 800-nm, 50-fs laser pulses at intensities of 5.4×10^{13} and 6.0×10^{13} W/cm^2.

of 68.1 or 53.1 ps for CH_3I or CH_3Br, respectively, where the molecules are maximum aligned along the pump-laser polarization. Typical time-of-flight mass spectra of CH_3I and CH_3Br molecules under an 800-nm laser with intensities of 5.4×10^{13} and 6.0×10^{13} W/cm^2 are shown in Fig. 3. The Keldysh parameter $\gamma \approx 1.2$ for these two molecules at the present laser intensities. The dominant peaks in the mass spectra are the CH_3X^+ parent ions and the fragments CH_3^+ and X^+.

The measured angular distributions of the parent and fragment ions from the ionization of CH_3I and CH_3Br molecules are shown in Fig. 4. The angular distribution shows a minimum at 0° and a maximum at 90° for parent ions CH_3I^+

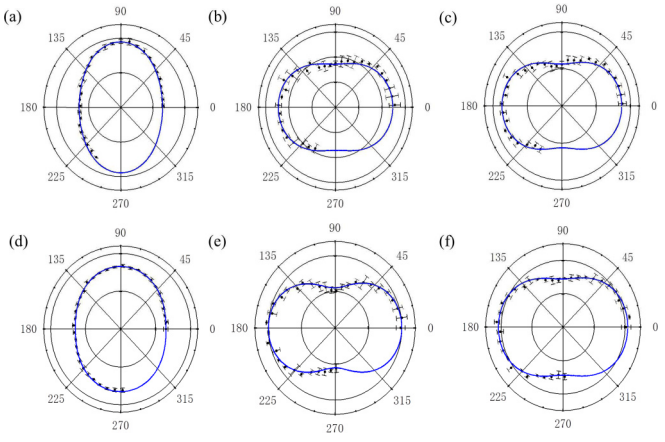

FIG. 4. Angular distribution of parent and fragment ions measured from the well-aligned molecular targets CH_3I and CH_3Br at the pump-probe delay time of 68.1 and 53.1 ps, respectively. Angular distributions for (a) CH_3I^+, (b) I^+, and (c) CH_3^+ and for (d) CH_3Br^+, (e) Br^+, and (f) CH_3^+. Error bars are estimated from the different experimental runs and blue lines are the fitted curves using Legendre polynomials $I = 1 + \sum \beta_{2i} P_{2i}$.

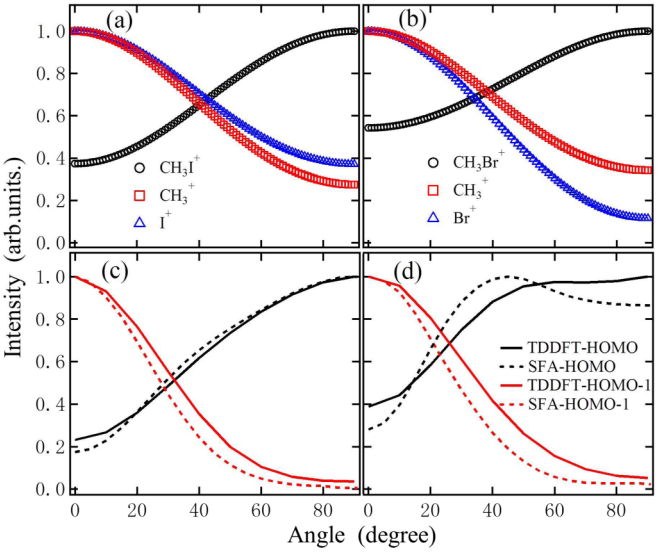

FIG. 5. Experimentally deconvolved angular-dependent ionization and dissociation probability S(θ) of CH_3X molecules, together with the MO-SFA and TDDFT calculation results. (a, b) Angular distributions of parent and fragment ions from CH_3I and CH_3Br (c, d) Angular distributions of HOMO (solid and dashed black lines) and HOMO-1 (solid and dashed red lines) orbitals from MO-SFA and TDDFT calculations for CH_3I and CH_3Br. Angular distributions are normalized at the maximum intensities.

and CH_3Br^+. However, the fragment ions show very different angular distributions, with a maximum at 0° and a minimum at 90°. In order to compare them with the theoretical calculation, the measured angular distributions of ions must be converted to the molecular frame from the experimental frame. The angular-dependent ionization and dissociation probabilities in the molecular frame, $S(\theta)$, are obtained from the deconvolution of the measured angular-dependent ion intensities, $M(\alpha)$, using the alignment distribution $A(\theta',\varphi')$ [12],

$$M(\alpha) = \int_{\varphi'=0}^{2\pi}\int_{\theta'=0}^{\pi} S[\theta(\theta',\varphi';\alpha)]A(\theta',\varphi')\sin(\theta')d\theta' d\varphi', \quad (9)$$

where θ' and φ' are the polar and azimuthal angles in the experimental frame with respect to the polarization axis of the aligning beam, and the angle θ is given by

$$\cos(\theta) = \cos(\alpha)\cos(\theta') - \sin(\alpha)\sin(\theta')\sin(\varphi'). \quad (10)$$

We expand the angular-dependent ionization and dissociation probabilities in terms of Legendre polynomials as $S(\theta) = \sum_{i=0}^{3} a_{2i} p_{2i} \cos(\theta)$. Figure 5 gives the angular-dependent ionization and dissociation probabilities $S(\theta)$ of these two molecules after deconvolution.

The results for the parent ions CH_3I^+ and CH_3Br^+, shown by the black circles in Figs. 5(a) and 5(b), are similar to the previous observations for OCS^+ [21]. This is because these molecules have similar HOMO distributions. In the case of CH_3X, the outer orbital of CH_3 becomes an orbital with a_1 symmetry in the C_{3v} point group and it combines with the n$p\sigma$ orbital of the halogen atom to give rise to a bonding-antibonding pair of A_1 orbitals and form nonbonding HOMOs [46]. It is expected that these degenerated HOMOs are close to

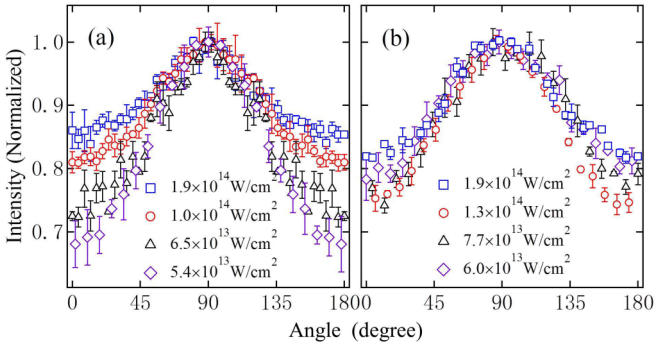

FIG. 6. Normalized angular distributions of parent ions for (a) CH_3I and (b) CH_3Br at different laser intensities.

an atomic p orbital, with the major character of the p electron distribution perpendicular to the C-X bonding axis. Therefore, it is reasonable to believe that the angular distribution of parent ions is maximum with the laser polarization perpendicular to the C-X bonding axis when strong-field ionization occurs and leads to the formation of CH_3X^+ in its electronic ground state X^2E [29]. We exclude the influence of excitation because the angular distributions of parent ions are similar with varying laser intensities as shown in Fig. 6. The parent ions should have different angular distributions considering that excited states have a laser-intensity-dependent population [47]. A trend of less anisotropic angular distributions appears with increasing laser intensity, due to the fact that more orbitals participate in the ionization process and the saturation effect under higher laser intensities. The ionization yield at 0^o will increase at higher laser intensities because of the contribution from the HOMO-1 [48]. Meanwhile the saturation effect will reduce the ionization signal at 90°. These effects will reduce the sharpness of the lobe in the measured angular distribution, as shown in Fig. 6. Furthermore, the distribution near 0° for CH_3I^+ is less than that for CH_3Br^+ [see Figs. 5(a) and 5(b)]. These distributions can be considered the contribution from HOMOs of non-p-electron character in the ionization. This interpretation is consistent with a recent calculation in which the contribution of the nonbonding p electron has been demonstrated to be different for different methyl halide molecules. The ionization is almost exclusively from the p orbital, with almost no contribution from the methyl group for CH_3I and with a nonnegligible contribution from the methyl group for CH_3Br [49].

For further interpretation of the measured angular distributions, calculated results based on the MO-SFA at length gauge (black lines) and the TDDFT (red lines) are presented in Figs. 5(c) and 5(d). It is found that in the case of CH_3I the angular distributions of the HOMO obtained from the TDDFT and SFA methods are almost the same as the experimental angular distribution of CH_3I^+, as shown by the black circles in Fig. 5(a). This supports that the main contribution is from HOMOs of a major np-orbital character during the formation of the parent ions of CH_3I^+. But in the case of CH_3Br^+, the discrepancies between the measured and the calculated angular distributions are obvious [see Figs. 5(b) and 5(d)] when the calculations consider HOMO electron ionization using the same theoretical approaches. This situation may come from the molecular orbital modification by the strong laser fields, which can affect the angular distribution of ionization significantly, as observed in the orientation-dependent high-harmonic generation of CH_3Br [28].

Measurement of the angular-dependent dissociation yields offers an opportunity to reveal the dissociation mechanisms [14–16,50]. Figures 5(a) and 5(b) also show the measured angular distributions of the fragment ions CH_3^+ (red squares) and X^+ (blue triangles) for CH_3I and CH_3Br, respectively. With the probe laser intensity at 5.4×10^{13} or 6.0×10^{13} W/cm^2, these fragment ions can be produced only from dissociation; no evidence has been observed of Coulomb explosion from multicharged parent ions (Fig. 3). Interestingly, these fragment ions show similar angular distributions after deconvolution, with a maximum at 0° and a minimum at 90°, the reverse of that of the parent ions. Also, the calculated results by MO-SFA or TDDFT for ionization of the HOMO-1 give similar angular distributions, as shown by red lines in Figs. 5(c) and 5(d) for CH_3I and CH_3Br, respectively, and the differences appearing at 90° may be caused by the HOMO contribution [11]. Thus, the present analyses suggest that the fragment ions of CH_3X (X = I, Br) are likely generated mainly from tunneling ionization of the HOMO-1. The present work indicates that the multiorbital contribution is important in understanding strong-field ionization of complex molecules. For the molecules CH_3X, this contribution can exert different influences with changing halogen atoms from I to Br. Measurement and reproduction of the angular distributions for either parent or fragment ions can provide sensitive orbital testing, as well as other dynamic effects. For these complex molecules, further theoretical developments and modeling are definitely required to fully establish this aspect.

IV. CONCLUSION

We have performed experimental measurements of angular-dependent ionization and dissociation yields of two polar molecules, CH_3X (X = I, Br), in strong laser fields. The obtained angular distributions suggest that the HOMO makes an important contribution to the production of parent ions. The dissociation mechanisms have been identified by comparing the measured angular distributions of fragment ions with theoretical calculations based on ionization from different molecular orbitals, and the agreement between experiment and theory indicates that the fragment ions are mainly generated from ionization of the molecules' HOMO-1. Experimental measurements and theoretical calculations on strong-field ionization and dissociation of polyatomic polar molecules will promote understanding of strong-field and attosecond science regarding complex polyatomic molecules.

ACKNOWLEDGMENT

This work was supported by National Basic Research Program of China (973 Program) Grant No. 2013CB922200 and the National Natural Science Foundation of China (Grants No. 11534004, No. 11627807, and No. 11704148).

[1] C. I. Blaga, J. Xu, A. D. DiChiara, E. Sistrunk, K. Zhang, P. Agostini, T. A. Miller, L. F. DiMauro, and C. D. Lin, Imaging ultrafast molecular dynamics with laser-induced electron diffraction, Nature (London) **483**, 194 (2012).

[2] M. Meckel, D. Comtois, D. Zeidler, A. Staudte, D. Pavicić, H. C. Bandulet, H. Pépin, J. C. Kieffer, R. Dörner, D. M. Villeneuve, and P. B. Corkum, Laser-induced electron tunneling and diffraction, Science **320**, 1478 (2008).

[3] J. Itatani, J. Levesque, D. Zeidler, H. Niikura, H. Pépin, J. C. Kieffer, P. B. Corkum, and D. M. Villeneuve, Tomographic imaging of molecular orbitals, Nature **432**, 867 (2004).

[4] C. Vozzi, M. Negro, F. Calegari, G. Sansone, M. Nisoli, S. De Silvestri, and S. Stagira, Generalized molecular orbital tomography, Nat. Phys. **7**, 822 (2011).

[5] C. Wu, C. Wu, D. Song, H. Su, Y. Yang, Z. Wu, X. Liu, H. Liu, M. Li, Y. Deng, Y. Liu, L. Peng, H. Jiang, and Q. Gong, Nonsequential and Sequential Fragmentation of CO_2^{3+} in Intense Laser Fields, Phys. Rev. Lett. **110**, 103601 (2013).

[6] J. Voigtsberger, S. Zeller, J. Becht, N. Neumann, F. Sturm, H.-K. Kim, W. Waitz, F. Trinter, M. Kunitski, A. Kalinin, J. Wu, W. Schöllkopf, D. Bressanini, A. Czasch, J. B. Willianms, K. Ullmann-Pfleger, L. Ph. H. Schmidt, M. S. Schöffler, R. E. Grisenti, T. Jahnke, and R. Dörner, Imaging the structure of the trimer systems $^4He_3$ and $^3He_4He_2$, Nat. Commun. **5**, 5765 (2014).

[7] Q. Wang, D. Wu, D. Zhang, M. Jin, F. Liu, H. Liu, Z. Hu, D. Ding, H. Mineo, Y. A. Dyakov, Y. Teranishi, S. D. Chao, A. M. Mebel, and S. H. Lin, Ionization and dissociation processes of pyrrolidine in intense femtosecond laser field, J. Phys. Chem. C **113**, 11805 (2009).

[8] M. Lezius, V. Blanchet, D. M. Rayner, D. M. Villeneuve, A. Stolow, and M. Y. Ivanov, Nonadiabatic Multielectron Dynamics in Strong Field Molecular Ionization, Phys. Rev. Lett. **86**, 51 (2001).

[9] A. E. Boguslavskiy, J. Mikosch, A. Gijsbertsen, M. Spanner, S. Patchkovskii, N. Gador, M. J. J. Vrakking, and A. Stolow, The multielectron ionization dynamics underlying attosecond strong-field spectroscopies, Science **335**, 1336 (2012).

[10] S. Petretti, Y. V. Vanne, A. Saenz, A. Castro, and P. Decleva, Alignment-Dependent Ionization of N_2, O_2, and CO_2 in Intense Laser Fields, Phys. Rev. Lett. **104**, 223001 (2010).

[11] H. Akagi, T. Otobe, A. Staudte, A. Shiner, F. Turner, R. Dörner, D. M. Villeneuve, and P. B. Corkum, Laser tunnel ionization from multiple orbitals in HCl, Science **325**, 1364 (2009).

[12] D. Pavičić, K. F. Lee, D. M. Rayner, P. B. Corkum, and D. M. Villeneuve, Direct Measurement of the Angular Dependence of Ionization for N_2, O_2, and CO_2 in Intense Laser Fields, Phys. Rev. Lett. **98**, 243001 (2007).

[13] R. Murray, M. Spanner, S. Patchkovskii, and M. Yu. Ivanov, Tunnel Ionization of Molecules and Orbital Imaging, Phys. Rev. Lett. **106**, 173001 (2011).

[14] X. Xie, K. Doblhoff-Dier, H. Xu, S. Roither, M. S. Schöffler, D. Kartashov, S. Erattupuzha, T. Rathje, G. G. Paulus, K. Yamanouchi, A. Baltuška, S. Gräfe, and M. Kitzler, Selective Control Over Fragmentation Reactions in Polyatomic Molecules Using Impulsive Laser Alignment, Phys. Rev. Lett. **112**, 163003 (2014).

[15] J. Wu, L. Ph. H. Schmidt, M. Kunitski, M. Meckel, S. Voss, H. Sann, H. Kim, T. Jahnke, A. Czasch, and R. Dörner, Multiorbital Tunneling Ionization of the CO Molecule, Phys. Rev. Lett. **108**, 183001 (2012).

[16] J. Mikosch, A. E. Boguslavskiy, I. Wilkinson, M. Spanner, S. Patchkovskii, and A. Stolow, Channel- and Angle-Resolved Above Threshold Ionization in the Molecular Frame, Phys. Rev. Lett. **110**, 023004 (2013).

[17] P. Sándor, A. Zhao, T. Rozgonyi, and T. Weinacht, Strong field molecular ionization to multiple ionic states: Direct versus indirect pathways, J. Phys. B **47**, 124021 (2014).

[18] A. Zhao, P. Sándor, T. Rozgonyi, and T. Weinacht, Removing electrons from more than one orbital: Direct and indirect pathways to excited states of molecular cations, J. Phys. B **47**, 204023 (2014).

[19] V. P. Majety and A. Scrinzi, Dynamic Exchange in the Strong Field Ionization of Molecules, Phys. Rev. Lett. **115**, 103002 (2015).

[20] L. Holmegaard, J. L. Hansen, L. Kalhϕj, S. L. Kragh, H. Stapelfeldt, F. Filsinger, J. Küpper, G. Meijer, D. Dimitrovski, M. Abu-samha, C. P. J. Martiny, and L. B. Madsen, Photoelectron angular distributions from strong-field ionization of oriented molecules, Nat. Phys. **6**, 428 (2010).

[21] J. L. Hansen, L. Holmegaard, J. H. Nielsen, H. Stapelfeldt, D. Dimitrovskiand, and L. B. Madsen, Orientation-dependent ionization yields from strong-field ionization of fixed-in-space linear and asymmetric top molecules, J. Phys. B **45**, 015101 (2012).

[22] L. B. Madsen, F. Jensen, O. I. Tolstikhin, and T. Morishita, Structure factors for tunneling ionization rates of molecules, Phys. Rev. A **87**, 013406 (2013).

[23] M. D. Śpiewanowski and L. B. Madsen, Alignment- and orientation-dependent strong-field ionization of molecules: Field-induced orbital distortion effects, Phys. Rev. A **91**, 043406 (2015).

[24] R. Johansen, K. G. Bay, L. Christensen, J. Thϕgersen, D. Dimitrovski, L. B. Madsen, and H. Stapelfeldt, Alignment-dependent strong-field ionization yields of carbonyl sulfide molecules induced by mid-infrared laser pulses, J. Phys. B **49**, 205601 (2016).

[25] H. Li, D. Ray, S. De, I. Znakovskaya, W. Cao, G. Laurent, Z. Wang, M. F. Kling, A. T. Le, and C. L. Cocke, Orientation dependence of the ionization of CO and NO in an intense femtosecond two-color laser field, Phys. Rev. A **84**, 043429 (2011).

[26] V. H. Hoang, S. F. Zhao, V. H. Le, and A. T. Le, Influence of permanent dipole and dynamic core-electron polarization on tunneling ionization of polar molecules, Phys. Rev. A **95**, 023407 (2017).

[27] B. Zhang, J. Yuan, and Z. Zhao, Dynamic Core Polarization in Strong-Field Ionization of CO Molecules, Phys. Rev. Lett. **111**, 163001 (2013).

[28] P. M. Kraus, O. I. Tolstikhin, D. Baykusheva, A. Rupenyan, J. Schneider, C. Z. Bisgaard, T. Morishita, F. Jensen, L. B. Madsen, and H. J. Wörner, Observation of laser-induced electronic structure in oriented polyatomic molecules, Nat. Commun. **6**, 7039 (2015).

[29] S. G. Walt, N. B. Ram, A. von Conta, O. I. Tolstikhin, L. B. Madsen, F. Jensen, and H. J. Wörner, Role of multielectron effects in the asymmetry of strong-field ionization and fragmentation of polar molecules: The methyl halide series, J. Phys. Chem. A **119**, 11772 (2015).

[30] L. He, J. Bulthuis, S. Luo, J. Wang, C. Lu, S. Stolte, D. Ding, and W. G. Roeterdink, Laser induced alignment of state-selected CH_3I, Phys. Chem. Chem. Phys. **17**, 24121 (2015).

[31] S. Luo, R. Zhu, L. He, W. Hu, X. Li, P. Ma, C. Wang, F. Liu, W. G. Roeterdink, S. Stolte, and D. Ding, Nonadiabatic laser-induced orientation and alignment of rotational-state-selected CH_3Br molecules, Phys. Rev. A **91**, 053408 (2015).

[32] S. Luo, W. Hu, J. Yu, R. Zhu, L. He, X. Li, P. Ma, C. Wang, F. Liu, W. G. Roeterdink, S. Stolte, and D. Ding, Rotational dynamics of quantum state-selected symmetric-top molecules in nonresonant femtosecond laser fields, J. Phys. Chem. A **121**, 777 (2017).

[33] W. C. Wallace, O. Ghafur, C. Khurmi, S. Sainadh U, J. E. Calvert, D. E. Laban, M. G. Pullen, K. Bartschat, A. N. Grum-Grzhimailo, D. Wells, H. M. Quiney, X. M. Tong, I. V. Litvinyuk, R. T. Sang, and D. Kielpinski, Precise and Accurate Measurements of Strong-Field Photoionization and a Transferable Laser Intensity Calibration Standard, Phys. Rev. Lett. **117**, 053001 (2016).

[34] T. K. Kjeldsen and L. B. Madsen, Strong-field ionization of N_2: Length and velocity gauge strong-field approximation and tunneling theory, J. Phys. B **37**, 2033 (2004).

[35] B. Zhang and Z. Zhao, Strong-field approximation for the ionization of N_2 and CO_2, Phys. Rev. A **82**, 035401 (2010).

[36] D. A. Telnov and S. I. Chu, Effects of electron structure and multielectron dynamical response on strong-field multiphoton ionization of diatomic molecules with arbitrary orientation: An all-electron time-dependent density-functional-theory approach, Phys. Rev. A **79**, 041401(R) (2009).

[37] M. R. Mack, D. Whitenack, and A. Wasserman, Exchange-correlation asymptotics and high harmonic spectra, Chem. Phys. Lett. **558**, 19 (2013).

[38] M. W. Schmidt, K. K. Baldridge, J. A. Boatz, S. T. Elbert, M. S. Gordon, J. H. Jensen, S. Koseki, N. Matsunaga, K. A. Nguyen, S. Su, T. L. Windus, M. Dupuis, and J. A. Montgomery Jr., General atomic and molecular electronic structure system, J. Comput. Chem. **14**, 1347 (1993).

[39] Y. Wang, S. Zhang, Z. Wei, and B. Zhang, Velocity map imaging of dissociative ionization and Coulomb explosion of CH_3I induced by a femtosecond laser, J. Phys. Chem. A **112**, 3846 (2008).

[40] X. Tang, X. Zhou, Z. Sun, S. Liu, F. Liu, L. Sheng, and B. Yan, Dissociation of internal energy-selected methyl bromide ion revealed from threshold photoelectron-photoion coincidence velocity imaging, J. Chem. Phys. **140**, 044312 (2014).

[41] L. Kleinman and D. M. Bylander, Efficacious Form for Model Pseudopotentials, Phys. Rev. Lett. **48**, 1425 (1982).

[42] S. Goedecker, M. Teter, and J. Hutter, Separable dual-space Gaussian pseudopotentials, Phys. Rev. B **54**, 1703 (1996).

[43] M. A. L. Marques, A. Castro, G. F. Bertsch, and A. Rubio, Octopus: A first-principles tool for excited electron ion dynamics, Comput. Phys. Commun. **151**, 60 (2003).

[44] A. Castro, H. Appel, M. Oliveira, C. A. Rozzi, X. Andrade, F. Lorenzen, M. A. L. Marques, E. K. U. Gross, and A. Rubio, Octopus: A tool for the application of time-dependent density functional theory, Phys. Status Solidi B **243**, 2465 (2006).

[45] R. Zhu, C. Wang, S. Luo, X. Yang, M. Zhang, F. Liu, and D. Ding, Role of rotational state-selected for nonadiabatic alignment: OCS molecules in femtosecond laser fields, Front. Phys. **8**, 236 (2013).

[46] G. O. Sullivan, The absorption spectrum of CH_3I in the extreme VUV, J. Phys. B **15**, L327 (1982).

[47] J. Yu, W. Hu, X. Li, P. Ma, L. He, F. Liu, C. Wang, S. Luo, and D. Ding, Contribution of resonance excitation on ionization of OCS molecules in strong laser fields, J. Phys. B **50**, 235602 (2017).

[48] L. He, Y. Pan, Y. Yang, S. Luo, C. Lu, H. Zhao, D. Li, L. Song, S. Stolte, D. Ding, and W. G. Roeterdink, Ion yields of laser aligned CH_3I and CH_3Br from multiple orbitals, Chem. Phys. Lett. **665**, 141 (2016).

[49] P. Hoerner and H. B. Schlegel, Angular dependence of strong field ionization of CH_3X (X = F, Cl, Br, or I) using time-dependent configuration interaction with an absorbing potential, J. Phys. Chem. A **121**, 5940 (2017).

[50] S. Luo, W. Hu, J. Yu, X. Li, L. He, C. Wang, F. Liu, and D. Ding, Multielectron effects in the strong field sequential ionization of aligned CH_3I molecules, J. Phys. Chem. A **121**, 6547 (2017).